Nanosecond Reversal of Three-Terminal Spin-Hall-Effect Memories Sustained at Cryogenic Temperatures

Graham E. Rowlands, Minh-Hai Nguyen, Sriharsha V. Aradhya, Shengjie Shi, Colm A. Ryan, Robert A. Buhrman, and Thomas A. Ohki

Phys. Rev. Applied **15**, L021004 — Published 25 February 2021

DOI: 10.1103/PhysRevApplied.15.L021004

Nanosecond Reversal of Three-Terminal Spin Hall Effect Memories Sustained at Cryogenic Temperatures

Graham E. Rowlands,[1, a)] Minh-Hai Nguyen,[2] Sriharsha V. Aradhya,[2] Shengjie Shi[2], Colm A. Ryan,[1] Robert A. Buhrman,[2] and Thomas A. Ohki[1]

[1)]Raytheon BBN Technologies, Cambridge, Massachusetts 02138

[2)]Cornell University, Ithaca, New York 14853

Abstract: *We characterize the nanosecond pulse switching performance of three-terminal magnetic tunnel junctions (MTJs) driven by the spin Hall effect (SHE), which persists at cryogenic temperatures owing to the considerable assistive torque from the Oersted field. These SHE-MTJ devices can be switched by current pulses as short as 1 ns with current densities $<10^{12}$ A/m^2 magnitude, exceeding expectations from conventional macrospin models. Furthermore, the pulse switching bit error rates remain below 10^{-6} for <10 ns pulses. With a realistic cryogenic memory cell in mind, we show that similar performance is achieved with exponentially decaying pulses expected to be delivered to the SHE-MTJ device by a nanocryotron device in a parallel configuration. These results suggest the viability of the SHE-MTJ structure as an element for high-performance general-purpose or application-specific superconducting computing systems.*

Introduction

After many years of steady progress, magnetoresistive random access memories (MRAMs) based on spin-transfer torque (STT) [1,2] switching are poised to complement and perhaps replace conventional DRAM architectures. One motivation for pursuing these novel architectures is their reduced static power consumption afforded by the intrinsic non-volatility of MRAM elements. Despite such a reduction, high-performance computing platforms will soon reach performance ceilings imposed by the power consumption of their underlying CMOS logic. As such, CMOS is being targeted for eventual replacement. This has caused a resurgent interest in Josephson junction (JJ) logic (an original competitor to CMOS), which could enable exascale computing at 1/100 the power of CMOS systems despite the power required for cooling the junctions below their superconducting transition temperature [3]. Such systems would require a fast cryogenic memory: preferably one that provides the same benefits offered by STT devices at room temperature. Superconducting electronics can also play a supporting role in other future computing technologies, in particular for facilitating quantum computing with superconducting qubits. These quantum processors will ultimately require a cryogenic control platform in order to scale beyond hundreds of qubits [4], obliging the waveform memory for control pulses to be kept in the same cryogenic environment. While notable progress has been made in creating memories that utilize both magnetic and superconducting effects [5], these devices are difficult to switch electrically and cannot presently leverage much of the extensive MRAM toolkit — synthetic antiferromagnets, pinning layers, etc. — given the adverse impacts of such structures on superconducting thin film circuits. We therefore restrict our attention to "normal" devices that operate by the same principles at room and cryogenic temperatures.

Anti-damping (AD) STT switching relies on advantageous thermal fluctuations to create an initial torque in devices with colinear in-plane magnetized (IPM) magnetic layers, and thus will operate neither quickly nor reliably at cryogenic temperatures. Accordingly, most demonstrations of low-temperature STT switching have utilized non-collinear spin torque from a perpendicular polarizer [6–8] or a canted in-plane polarizer [9] to increase the initial STT (as has been done at room temperature [10–12]). Recently it was demonstrated that three-terminal magnetic tunnel junctions (MTJs) based on the spin-Hall effect [13,14] (sometimes referred to as spin-orbit torque MRAM devices or SOT-MRAM [15] when switching is presumed to be driven by the

Rashba-Edelstein interaction [16]) do not suffer from these limitations, possibly because of the non-uniform nature of the magnetic reversal [17] in combination with the beneficial in-plane Oersted field generated by the write current in the spin Hall channel [18]. Remarkably, it has been demonstrated that SHE-MTJs devices can be switched with sub-ns pulses and can exhibit write error rates (WERs) below 10^{-5} for pulses as short as 2 ns without fear of dielectric tunnel barrier breakdown [19]. This IPM approach offers considerable simplicity compared to spin-torque device alternatives: precessional switching in multi-polarizer devices requires very precise timing inherent to precessional reversal dynamics [8,20], while fast SHE/SOT switching of a perpendicular magnetized (PM) free layer requires some manner of in-plane effective-field bias (from exchange pinning, external fields, or other mechanisms) to break the axial symmetry of the FL, as well as precise pulse timing in the short pulse regime to obtain deterministic reversal [7]. Here we demonstrate that IPM SHE-MTJs continue to provide reliable and fast switching behavior down to $T = 3$ K without the need for these additional complexities. We examine the potential compatibility of these devices with write pulses from superconducting nano-cryotron (nTron) drivers [21], finding an unexpected performance improvement.

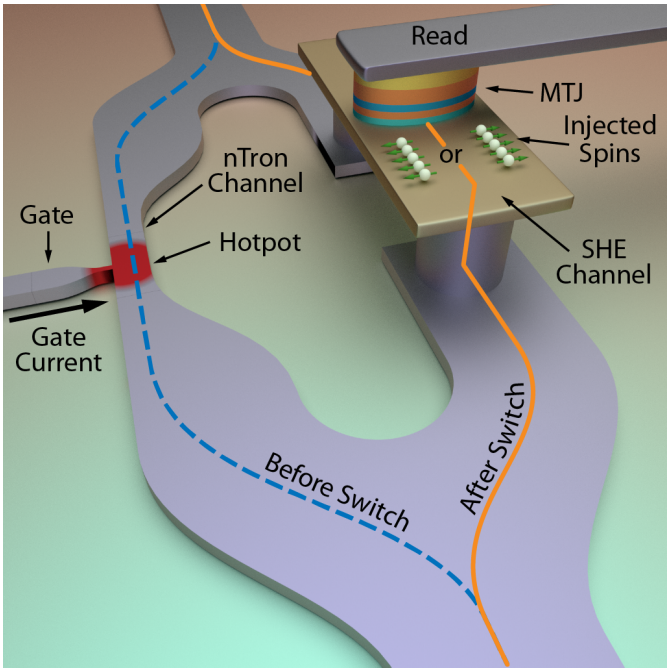

Figure 1: *Schematic of the proposed memory unit cell with an nTron select element and SHE-MTJ element. Current flows through the nTron channel but can be redirected through the spin Hall channel by the application of a gate current that*

creates a hotspot in the indicated area. Spins with either indicated orientation are created by reversing the polarity of the current through the unit cell.

Device Design

Our devices consist of an IPM MTJ patterned into an elliptical nanopillar on top of a 200 nm wide Pt(5)/Hf(0.7) spin-Hall channel (thicknesses in nm). The choice of Pt is motivated by its positive spin-Hall angle, θ_{SH}, for which the in-plane Oersted field from the write current in the spin Hall channel assists the torque from the SHE. The result is fast reversal with minimal incubation delay [18]. The long axis of the ellipse defines the magnetic easy axis of the free layer (FL), and it is oriented perpendicular to the spin Hall channel in order that it is aligned with the spin accumulation therein. The Hf spacer reduces the undesired interfacial enhancement of the magnetic damping of the FL arising from the interaction of Pt with the ferromagnetic material, without causing a significant detrimental effect on the effective spin torque efficiency ξ_{SH} [22]. The FL is composed of $Fe_{60}Co_{20}B_{20}$ (1.6), and is subject to a perpendicular magnetic anisotropy field of approximately 1 T originating from the MgO/FeCoB interface [23]. This anisotropy field partially compensates the demagnetizing field of the FL — resulting in a reduced effective magnetization — but is insufficient to cause the FL to orient out of the plane. Despite any anisotropy or saturation magnetization variations with temperature, the FL remains in-plane from T = 3 K to T = 300 K. The reference layer (RL) consists of a FeCoB/Ru/FeCoB synthetic antiferromagnet (SAF) strongly exchange pinned by IrMn in order to minimize polarity dependent switching behavior. Full device details are given in our previous work [17].

A schematic of our proposed memory cell is shown in Fig. 1. The SHE-MTJs cannot be driven directly by JJ logic, which operates at the level of individual flux quanta. Instead, we will utilize nTron devices as select elements that are triggered by gate pulses from peripheral JJ logic. The gate pulses nucleate a hot-spot in the nTron channel constriction, causing it to enter the normal state and develop a resistance that is engineered to reach many kΩs [24]. Current is thereby redirected to write the SHE-MTJ, though some fraction of the current is dissipated in the nTron channel. The efficiency of this redirection can be improved greatly with more advanced fabrication processes that reduce the lead resistance to the SHE-MTJ. For this work we study isolated memory elements using a fast switching measurement setup that can emulate the current

redirection from the nTron. All measurements reported in this paper were performed at 3 K in a cryogenic environment described elsewhere [25].

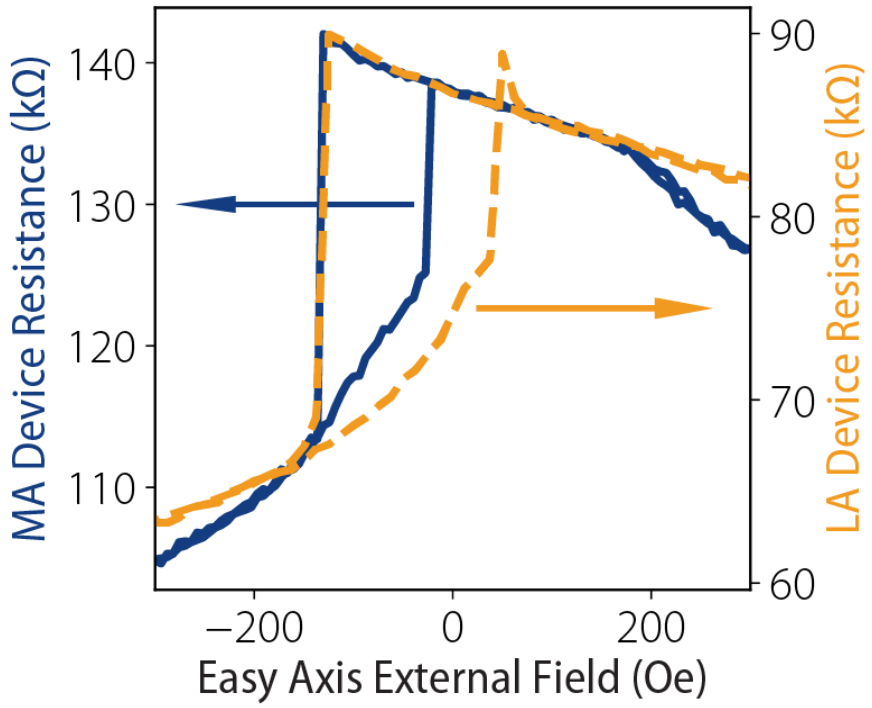

Figure 2: *Magnetic minor loops of a MA (left axis) and LA (right axis) SHE-MTJ device, showing a sharp AP→P switching but a gradual P→AP transition which can be attributed to the Néel coupling between the magnetic edge charges of the reference and free layer, and/or the complex multidomain micromagnetic reversal.*

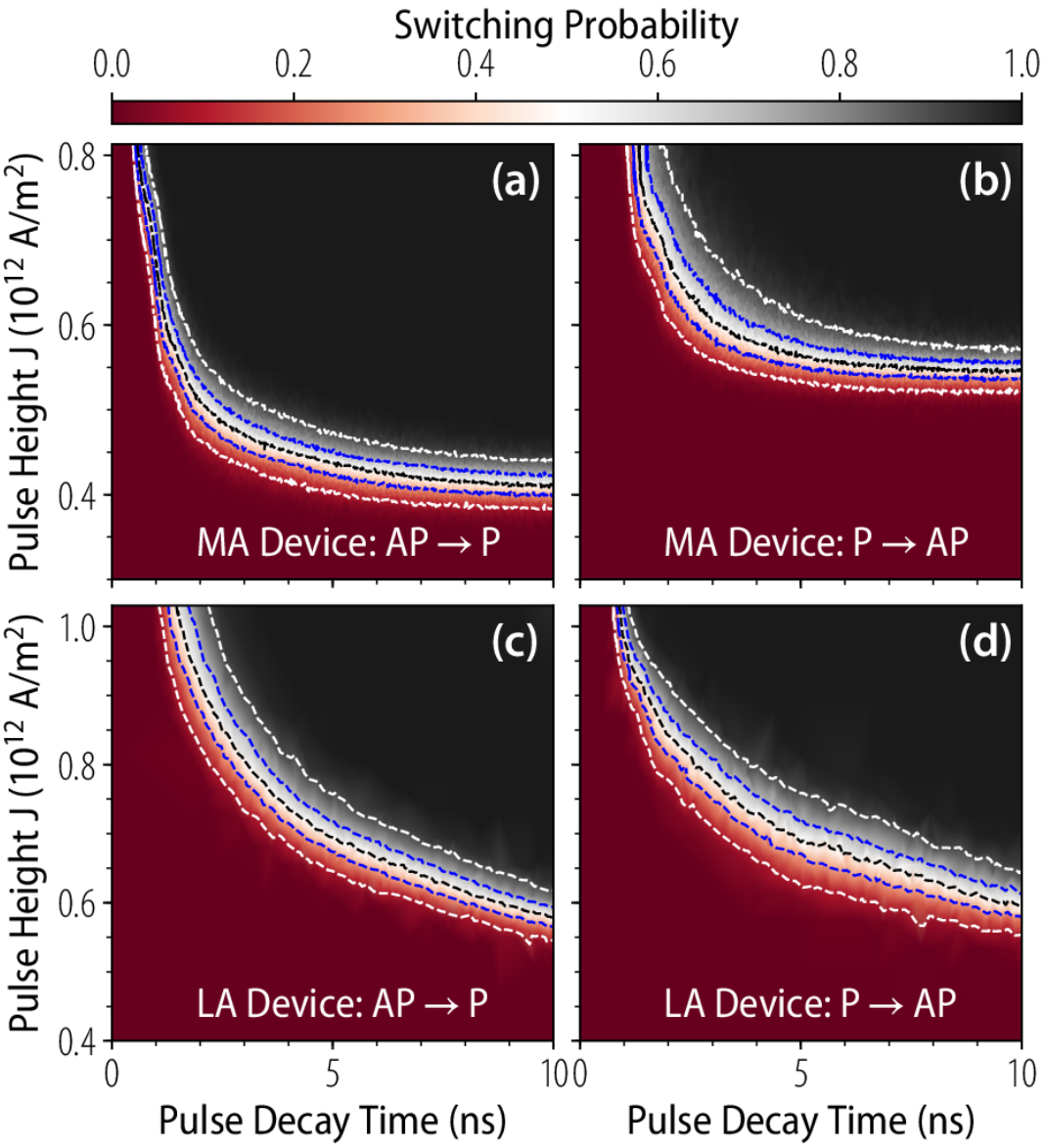

Figure 3: *Phase diagrams for an (a,b) MA device and an (c,d) LA device switching in the (a,c) AP→P and (b,d) P→AP polarities. Color encodes the probability as shown at the top of the figure. The black dotted line shows the 50% probability boundary, while the blue and white dotted lines show* $\pm 20\%$ *and* $\pm 40\%$ *from the* $\pm 50\%$ *boundary, respectively. The image is composed of triangular elements drawn with a linear color-scale interpolation. Each vertex is the result of approximately 1024 switching attempts.*

Device Operation

We measured the easy axis minor magnetic hysteresis loops of a standalone SHE-MTJ device using a superconducting coil pair, thereafter biasing the devices with an offset field that puts them in the bistable region supporting both parallel (P) and antiparallel (AP) resistance states. This offset field was required since we have not yet optimized the SAF reference layer to reduce the fringing field seen by the FL. Two types of elliptical nanopillar samples were measured, those with a medium aspect (MA) ratio (nominally: 115nm x 45 nm) and those with a low aspect (LA) ratio (nominally: 115 nm x 70 nm). In Fig. 2, we show the minor loops for the field switching of the free layer of a MA and LA device. We observe sharp AP→P switching, but a curvature in the P→AP transition that we attribute to the Néel coupling between the two magnetic layers [26], and/or to the complex multidomain micromagnetic reversal process, as studied by simulation in [18], due at least in part to edge roughness.

We determined the approximate thermal stability factors $\Delta(T)(\equiv E_a/k_BT)$ of the LA and MA devices by applying shallow pulses in the soft write-error regime [27], finding $\Delta_{\mathrm{MA}}(3\mathrm{K}) = 102 \pm 2$ and $\Delta_{\mathrm{LA}}(3\mathrm{K}) = 55 \pm 6$. (Here E_a is the thermal activation energy for magnetic reversal.) We then performed short pulse switching attempts at an attempt rate of 1 kHz, actively resetting the device with an inverted current pulse after each repetition.

The resulting switching phase diagrams (SPDs) are shown in Fig. 3(a-d) as a function of current density J and pulse duration τ. We used an adaptive measurement technique that iteratively refines a Delaunay triangulation [28] across the measurement coordinates, allowing us to acquire an accurate phase diagram with many fewer points than are required for a rectilinear sweep. The SPDs demonstrate that for each polarity and pillar aspect ratio there is a region of highly successful switching (black). For the MA device there is a substantial difference in the current required to reach the 50% probability boundary (black dotted line) between AP→P and P→AP polarities. In the LA device this is much less evidence. In all four cases the complex variation of the phase boundary, including its width, cannot be explained expected by rigid domain macrospin modeling. This behavior is consistent with micromagnetic simulations [18] which show that in the strong, short-pulse regime the reversal proceeds by a non-uniform process involving the formation and propagation of one or more sub-domains within the free layer (similarly nonuniform reversal have been directly imaged in PM free layers driven by

SOT [29,30]). The initial magnetization profiles and the sign of the spin Hall angle are central to the details of this reversal. The FL and RL energetically prefer an AP alignment, and are uniformly saturated opposite one another in the AP state. In the P-state, they scissor away from one another to reduce the dipolar energy, creating a significant curvature. Without accounting for the Oersted field, the nature of current-induced reversal is notably different in both of these cases, with the P→AP reversal taking place via a slow multi-domain process and the AP→P reversal proceeding more quickly. The inclusion of the Oersted field reduces this imbalance if the channel has a positive spin Hall angle (assisting the spin-torque), making the P→AP switching proceed in a more uniform manner. On the other hand, it hinders performance for both switching polarities if the channel has a negative spin Hall angle (impeding the spin-torque) [18]. The sign of the spin Hall angle — not just its magnitude — is therefore important in determining the high-speed operability of in-plane SOT-MRAM. In Figs. 3(c-d) our LA samples show similar switching currents and timescales for both polarities, consistent with an assistive Oersted field that expedites and stabilizes coherent switching. Meanwhile, In Figs. 3(a-b) our MA sample's P→AP switching is clearly inhibited. This is likely caused by its very high energy barrier (twice that of the LA device), which leaves switching to proceed via slow and non-uniform multi-domain nucleation processes. In this case, the Oersted field confers minimal benefit since it is too small to stabilize coherent reversal. Field-like torque contributions from SHE or SOT could be an additional source of torque [31,32], but we do not attempt to disentangle their potential contributions in this work.

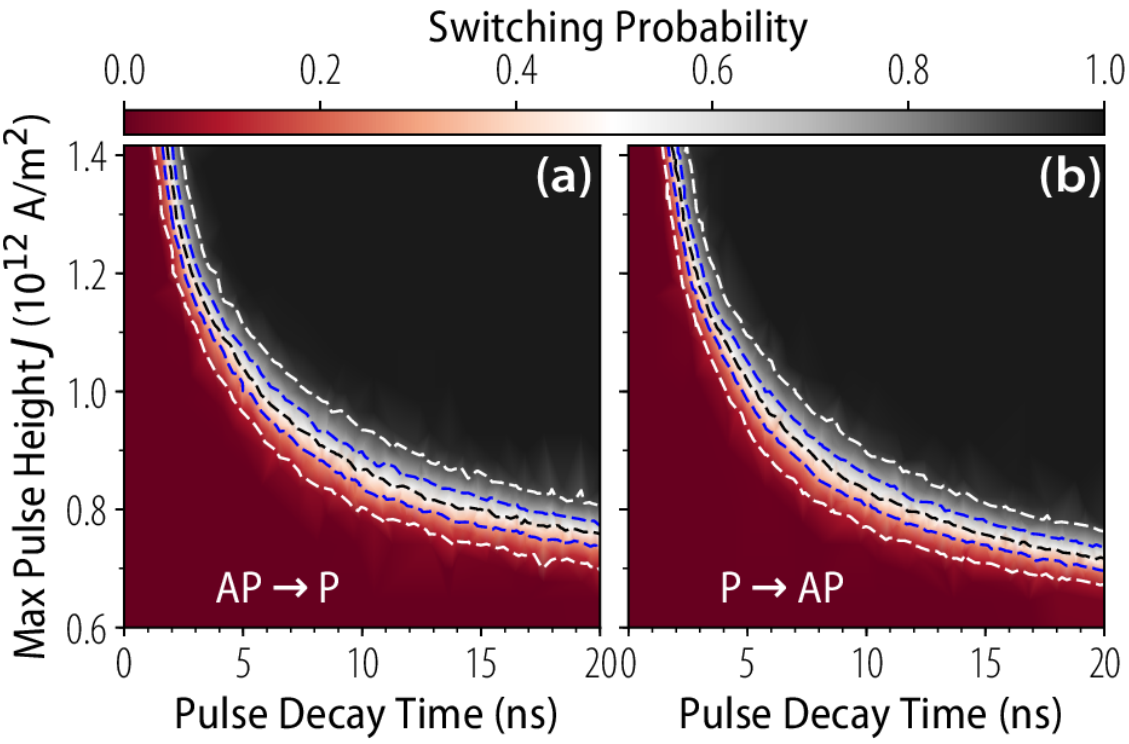

Figure 4: *Phase diagrams for a LA device subject to nTron-like pulses of (a) AP→P and (b) P→AP polarities. The left axes give the peak value of the current density J. The meaning of the dotted lines is described in Fig. 3.*

In the circuit of Fig. 1 the write current flows through the SHE-MTJ channel with an exponentially decaying profile in time. For traditional AD devices this presents complications: the initial energy from the write pulse is squandered given the collinearity of spin-torque and the lack of thermally induced deflection of the FL. We expect better performance in the SHE-MTJ devices, however, given their Oersted-field assisted switching, and use a Keysight M8190A Arbitrary Waveform Generator (AWG) to stimulate our devices with exponentially decaying write pulses. We measure the switching phase-diagrams for our LA devices (Fig. 4), this time in terms of the pulses' peak current J and $1/e$ decay time. The switching phase boundaries remain well-defined, and show an unexpected decrease in the polarity asymmetry observed in the rectangular phase diagrams (Fig. 3(a-b)). Both the positions and profiles of the phase boundaries converge: the P→AP profile becomes narrower at longer timescales and the AP→P profile becomes narrower at short timescales. We conclude that STT during the exponential tail is likely

responsible for coaxing the FL magnetization into its final state and reducing the width of the phase boundaries.

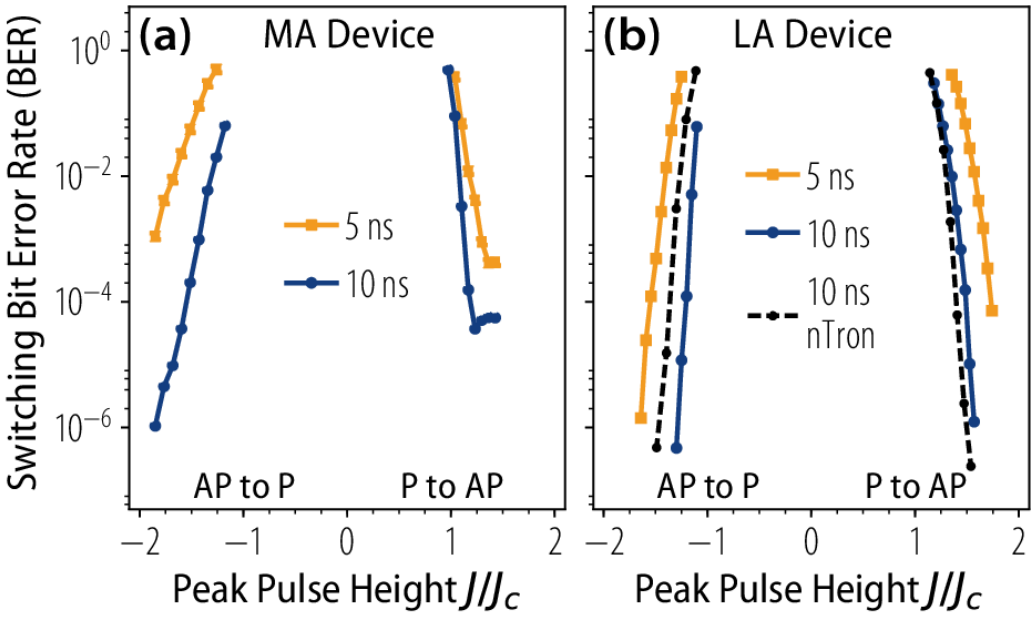

Figure 5: *Summary of the bit error rates (BERs) for LA devices. Peak pulse heights are normalized by the J_c corresponding to their particular polarity and pulse envelope (rectangular or exponentially decaying).*

Finally, we examined the bit error rate (BER) of our devices. We applied an number of switching pulses that yielded a switching probability at least two standard deviations above the statistical floor of our data (as determined by fitting to a β-distribution.) For time considerations, measurements were terminated once a BER of $\leq 10^{-6}$ and the results here are not indicative of any device limitations. The BER for an LA device shown in Fig. 5 shows a sharp falloff of the for both switching polarities; 10 ns rectangular pulses easily provide polarity-independent error rates of $< 10^{-6}$ for $J < 2J_c$. For 5 ns rectangular pulses, the LA devices start to exhibit some polarity dependence and suffer from a higher P→AP BER. The dotted line in Fig. 5 shows that the nTron-like pulses can produce similarly low error rates, easily reaching our self-imposed limit of $< 10^{-6}$. This means that our intended memory cell (Fig. 1) is well suited to the stimulus requirements of the SHE-MTJs.

Conclusions

In closing, we have shown that SHE-MTJ devices can operate at cryogenic temperature with fast switching speeds ($\tau_0 \approx 1$ ns) and high reliability (BERs $< 10^{-6}$). As we previously observed at room temperature, this behavior is consistent with an assistive torque provided by the Oersted field [18]. It appears that an incubation delay can still be avoided in the low temperature regime, owing to the non-collinearity of this additional initial torque. These results affirm the advantages of Pt-based SHE-MTJ systems. We expect that further improvements in switching uniformity, speed, and BER could be obtained by utilizing devices whose Δ values are tuned to be < 40 at $T \approx 3$ K. For such Δ values, one obtains a balance between memory retention times and the ease of switching. We also found that nTron-like switching pulses are surprisingly effective: their large initial amplitudes would be wasted were switching to proceed via the anti-damping spin torque alone. With these shaped pulses, we obtain polarity-independent switching with BERs that taper off rapidly to $< 10^{-6}$. We expect that these memory devices will play an important role in cryogenic computing environments: serving as a main memory for general-purpose superconducting computing architectures or in specific applications such as waveform memory for superconducting qubit control platforms.

Acknowledgements

The research is based upon work supported by the Office of the Director of National Intelligence (ODNI), Intelligence Advanced Research Projects Activity (IARPA), via contract W911NF-14-C0089. The views and conclusions contained herein are those of the authors and should not be interpreted as necessarily representing the official policies or endorsements, either expressed or implied, of the ODNI, IARPA, or the U.S. Government. The U.S. Government is authorized to reproduce and distribute reprints for Governmental purposes notwithstanding any copyright annotation thereon. Additionally, this work was supported by the Office of Naval Research, by the NSF/MRSEC program (DMR-1120296) through the Cornell Center for Materials Research, and by the NSF (Grant No. ECCS-0335765) through use of the Cornell Nanofabrication Facility/National Nanofabrication Infrastructure Network.

Methods

Samples are measured in a cryogen-free HPD cryo-probe station using microwave probes connected to lines thermalized by 0 dB attenuators at each stage. We confirmed that thermal

noise from the ambient environment does not have an appreciable effect on our studies. Write pulses are delivered by a combination of a PSPL 10,070A pulse generator with 2.5 ps time resolution and a Keysight M8190A 12GS arbitrary waveform generator. The former is passed through a voltage-controlled attenuator giving precise voltage control rather than relying on coarse 1 dB step attenuators. The instruments' outputs are combined by a 180° hybrid before being routed to the cryostat.

Each switching pulses is preceded by a 10 ns, ~1×10^{12} A/m^2 reset pulse that initializes the magnetization. The MTJ state is measured before and after each switching pulse with a sense current of 3 μA. We discard any attempts where resetting was unsuccessful. In the switching phase diagrams of Figs. 3-4, the probability is given as the expectation value of the beta-distribution constructed from 1024 switching attempts. The BERs shown in Fig. 5 are determined in the same manner, but the number of attempts was adaptively chosen to maintain a confidence interval of 95% based on the beta distribution.

Our measurements are performed using our freely available Auspex and Adapt packages available at github.com/BBN-Q.

References

[1] J. C. Slonczewski, *Current-Driven Excitation of Magnetic Multilayers*, Journal of Magnetism and Magnetic Materials **159**, L1 (1996).

[2] L. Berger, *Emission of Spin Waves by a Magnetic Multilayer Traversed by a Current*, Physical Review B **54**, 9353 (1996).

[3] D. S. Holmes, A. L. Ripple, and M. A. Manheimer, *Energy-Efficient Superconducting Computing—Power Budgets and Requirements*, IEEE Transactions on Applied Superconductivity **23**, 1701610 (2013).

[4] R. McDermott, M. G. Vavilov, B. L. T. Plourde, F. K. Wilhelm, P. J. Liebermann, O. A. Mukhanov, and T. A. Ohki, *Quantum-Classical Interface Based on Single Flux Quantum Digital Logic*, Quantum Science and Technology **3**, (2018).

[5] E. C. Gingrich, B. M. Niedzielski, J. A. Glick, Y. Wang, D. L. Miller, R. Loloee, W. P. P. Jr, and N. O. Birge, *Controllable 0 – π Josephson Junctions Containing a Ferromagnetic Spin Valve*, 1 (2016).

[6] O. J. Lee, V. S. Pribiag, P. M. Braganca, P. G. Gowtham, D. C. Ralph, and R. A. Buhrman, *Ultrafast Switching of a Nanomagnet by a Combined Out-of-Plane and in-Plane Polarized Spin Current Pulse*, Applied Physics Letters **95**, 012506 (2009).

[7] J. Park, D. C. Ralph, and R. A. Buhrman, *Fast Deterministic Switching in Orthogonal Spin Torque Devices via the Control of the Relative Spin Polarizations*, Applied Physics Letters **103**, 252406 (2013).
[8] G. E. Rowlands, C. A. Ryan, L. Ye, L. Rehm, D. Pinna, A. D. Kent, and T. A. Ohki, *A Cryogenic Spin-Torque Memory Element with Precessional Magnetization Dynamics*, Scientific Reports **9**, 803 (2019).
[9] I. N. Krivorotov, N. C. Emley, J. C. Sankey, S. I. Kiselev, D. C. Ralph, and R. A. Buhrman, *Time-Domain Measurements of Nanomagnet Dynamics Driven by Spin-Transfer Torques.*, Science (New York, N.Y.) **307**, 228 (2005).
[10] H. Liu, D. Bedau, D. Backes, J. A. Katine, J. Langer, and a. D. Kent, *Ultrafast Switching in Magnetic Tunnel Junction Based Orthogonal Spin Transfer Devices*, Applied Physics Letters **97**, 242510 (2010).
[11] G. E. Rowlands, T. Rahman, J. A. Katine, J. Langer, A. Lyle, H. Zhao, J. G. Alzate, A. A. Kovalev, Y. Tserkovnyak, Z. M. Zeng, H. W. Jiang, K. Galatsis, Y. M. Huai, P. K. Amiri, K. L. Wang, I. N. Krivorotov, and J. Wang, *Deep Subnanosecond Spin Torque Switching in Magnetic Tunnel Junctions with Combined In-Plane and Perpendicular Polarizers*, Applied Physics Letters **98**, 102509 (2011).
[12] C. Papusoi, B. Delaët, B. Rodmacq, D. Houssameddine, J.-P. Michel, U. Ebels, R. C. Sousa, L. D. Buda-Prejbeanu, and B. Dieny, *100 Ps Precessional Spin-Transfer Switching of a Planar Magnetic Random Access Memory Cell With Perpendicular Spin Polarizer*, Applied Physics Letters **95**, 072506 (2009).
[13] L. Liu, T. Moriyama, D. C. Ralph, and R. A. Buhrman, *Spin-Torque Ferromagnetic Resonance Induced by the Spin Hall Effect*, Phys. Rev. Lett. **106**, 036601 (2011).
[14] L. Liu, C.-F. Pai, Y. Li, H. W. Tseng, D. C. Ralph, and R. A. Buhrman, *Spin-Torque Switching with the Giant Spin Hall Effect of Tantalum*, Science **336**, 555 (2012).
[15] M. Cubukcu, O. Boulle, M. Drouard, K. Garello, C. Onur Avci, I. Mihai Miron, J. Langer, B. Ocker, P. Gambardella, and G. Gaudin, *Spin-Orbit Torque Magnetization Switching of a Three-Terminal Perpendicular Magnetic Tunnel Junction*, Appl. Phys. Lett. **104**, 042406 (2014).
[16] I. Mihai Miron, G. Gaudin, S. Auffret, B. Rodmacq, A. Schuhl, S. Pizzini, J. Vogel, and P. Gambardella, *Current-Driven Spin Torque Induced by the Rashba Effect in a Ferromagnetic Metal Layer*, Nature Mater **9**, 230 (2010).
[17] S. V. Aradhya, G. E. Rowlands, J. Oh, D. C. Ralph, and R. A. Buhrman, *Nanosecond-Timescale Low Energy Switching of In-Plane Magnetic Tunnel Junctions through Dynamic Oersted-Field-Assisted Spin Hall Effect*, Nano Letters **16**, 5987 (2016).
[18] G. E. Rowlands, S. V. Aradhya, S. Shi, E. H. Yandel, J. Oh, D. C. Ralph, and R. A. Buhrman, *Nanosecond Magnetization Dynamics during Spin Hall Switching of In-Plane Magnetic Tunnel Junctions*, Appl. Phys. Lett. **110**, 122402 (2017).
[19] S. Shi, Y. Ou, S. V. Aradhya, D. C. Ralph, and R. A. Buhrman, *Fast Low-Current Spin-Orbit-Torque Switching of Magnetic Tunnel Junctions through Atomic Modifications of the Free-Layer Interfaces*, Physical Review Applied **9**, 11002 (2018).
[20] J. Park, G. E. Rowlands, O. J. Lee, D. C. Ralph, and R. A. Buhrman, *Macrospin Modeling of Sub-Ns Pulse Switching of Perpendicularly Magnetized Free Layer via Spin-Orbit Torques for Cryogenic Memory Applications*, Applied Physics Letters **105**, 102404 (2014).
[21] A. N. McCaughan and K. K. Berggren, *A Superconducting-Nanowire Three-Terminal Electrothermal Device*, Nano Letters **14**, 5748 (2014).

[22] M.-H. Nguyen, C.-F. Pai, K. X. Nguyen, D. A. Muller, D. C. Ralph, and R. A. Buhrman, *Enhancement of the Anti-Damping Spin Torque Efficacy of Platinum by Interface Modification*, Applied Physics Letters **106**, 222402 (2015).
[23] S. Ikeda, K. Miura, H. Yamamoto, K. Mizunuma, H. D. Gan, M. Endo, S. Kanai, J. Hayakawa, F. Matsukura, and H. Ohno, *A Perpendicular-Anisotropy CoFeB–MgO Magnetic Tunnel Junction*, Nature Mater **9**, 721 (2010).
[24] M.-H. Nguyen, G. J. Ribeill, M. V. Gustafsson, S. Shi, S. V. Aradhya, A. P. Wagner, L. M. Ranzani, L. Zhu, R. Baghdadi, B. Butters, E. Toomey, M. Colangelo, P. A. Truitt, A. Jafari-Salim, D. McAllister, D. Yohannes, S. R. Cheng, R. Lazarus, O. Mukhanov, K. K. Berggren, R. A. Buhrman, G. E. Rowlands, and T. A. Ohki, *Cryogenic Memory Architecture Integrating Spin Hall Effect Based Magnetic Memory and Superconductive Cryotron Devices*, Sci Rep **10**, 248 (2020).
[25] M.-H. Nguyen, The Spin Hall Effect in Platinum/Ferromagnet Multilayers and Its Application in Three-Terminal Magnetic Tunnel Junction Structures, Cornell University, 2017.
[26] G. D. Fuchs, N. C. Emley, I. N. Krivorotov, P. M. Braganca, E. M. Ryan, S. I. Kiselev, J. C. Sankey, D. C. Ralph, R. A. Buhrman, and J. A. Katine, *Spin-Transfer Effects in Nanoscale Magnetic Tunnel Junctions*, Applied Physics Letters **85**, 1205 (2004).
[27] R. Heindl, W. H. Rippard, S. E. Russek, M. R. Pufall, and A. B. Kos, *Validity of the Thermal Activation Model for Spin-Transfer Torque Switching in Magnetic Tunnel Junctions*, Journal of Applied Physics **109**, 073910 (2011).
[28] B. Delaunay, *Sur La Sphère Vide. A La Mémoire de Georges Voronoï*, Bulletin de l'Académie Des Sciences de l'URSS. Classe Des Sciences Mathématiques et Na 793 (1934).
[29] M. Baumgartner, K. Garello, J. Mendil, C. O. Avci, E. Grimaldi, C. Murer, J. Feng, M. Gabureac, C. Stamm, Y. Acremann, S. Finizio, S. Wintz, J. Raabe, and P. Gambardella, *Spatially and Time-Resolved Magnetization Dynamics Driven by Spin–Orbit Torques*, Nature Nanotech **12**, 980 (2017).
[30] M. M. Decker, M. S. Wörnle, A. Meisinger, M. Vogel, H. S. Körner, G. Y. Shi, C. Song, M. Kronseder, and C. H. Back, *Time Resolved Measurements of the Switching Trajectory of Pt / Co Elements Induced by Spin-Orbit Torques*, Phys. Rev. Lett. **118**, 257201 (2017).
[31] P. M. Haney, H.-W. Lee, K.-J. Lee, A. Manchon, and M. D. Stiles, *Current Induced Torques and Interfacial Spin-Orbit Coupling: Semiclassical Modeling*, Phys. Rev. B **87**, 174411 (2013).
[32] K.-W. Kim, S.-M. Seo, J. Ryu, K.-J. Lee, and H.-W. Lee, *Magnetization Dynamics Induced by In-Plane Currents in Ultrathin Magnetic Nanostructures with Rashba Spin-Orbit Coupling*, Phys. Rev. B **85**, 180404 (2012).